

# Imaging Ultrafast Dynamical Diffraction wavefronts of femtosecond laser-induced lattice distortions inside crystalline semiconductors

Angel Rodríguez-Fernández,\* Jan-Etienne Pudell, Roman Shayduk, Wonhyuk Jo, James Wrigley, Johannes Möller, Peter Zalden, Alexey Zozulya, Jörg Hallmann, and Anders Madsen  
*European XFEL Facility GmbH, Holzkoppel 4, Schenefeld DE, 22869*

Pablo Villanueva-Perez

*Division of Synchrotron Radiation Research and NanoLund,  
 Department of Physics, Lund University, Lund, 22100 Sweden*

Zdenek Matej

*MAX IV Laboratory, Lund University, Lund, Sweden SE-22100*

Thies J. Albert, Dominik Kaczmarek, and Klaus Sokolowski-Tinten

*Department of Physics, Universitt Duisburg-Essen,  
 Lotharstr. 1, 47057 Duisburg, Germany. and  
 Center for Nanointegration Duisburg-Essen, Universität Duisburg-Essen,  
 Carl-Benz-Str. 199, 47057 Duisburg, Germany*

Antonowicz Jerzy

*Faculty of Physics, Warsaw University of Technology,  
 Koszykowa 75, 00-662 Warsaw, Poland*

Oleksii I. Liubchenko, Rahimi Mosafer, Ryszard Sobierajski, Javier Solis, and Jan Siegel<sup>†</sup>

*Laser Processing Group, Instituto de Optica (IO-CSIC),  
 Consejo Superior de Investigaciones Científicas, CSIC, 28006, Madrid, Spain*

(Dated: April 4, 2025)

# Abstract

Material processing with femtosecond lasers has attracted enormous attention because of its potential for technology and industrial applications. In parallel, time-resolved x-ray diffraction has been successfully used to study ultrafast structural distortion dynamics in semiconductor thin films or surface layers of bulk materials. However, 'real-world' processing applications deal mostly with bulk materials, which prevents the use of such techniques. For processing applications, a fast and depth-sensitive probe is needed. To address this, we present a novel technique based on ultrafast dynamical diffraction (UDD) capable of imaging transient strain distributions inside bulk crystals upon single-pulse excitation. This pump-probe technique provides a complete picture of the temporal evolution of ultrafast distortion depth profiles. Our measurements were obtained in a thin crystalline Si wafer upon single pulse femtosecond optical excitation revealing that below the melting threshold strong lattice distortions appear on picosecond time scales due to the formation and propagation of strain waves into the bulk.

Keywords: Imaging, Ultrafast, Crystal Distortions, Laser, Dynamical Diffraction, XFEL

## I. INTRODUCTION

In the last decades, the countless potential applications in technology and industry have further enhanced the strong interest in the use of ultrafast lasers for material processing. One key aspect is the reduced thermal load, enabling the fabrication of smaller and sharper feature sizes, even below the diffraction limit, as well as enabling surface and sub-surface processing of transparent materials due to non-linear absorption mechanisms [1, 2]. This advantage can be implemented by using laser pulses that are shorter than the time it takes for the strongly excited electron subsystem to transfer its energy to the lattice (typically a few picosecond). Such pulses can generate highly non-equilibrium states and trigger structural changes within a few hundred femtoseconds [3], as confirmed experimentally using time-resolved x-ray diffraction for the case of non-thermal melting in semiconductors [4–6].

One of the limitations of conventional time-resolved x-ray diffraction techniques is that the diffraction signal recorded by the detector is an average over a depth of the order of

---

\* Contact author: angel.rodriquez-fernandez@xfel.eu

† Contact author: j.siegel@io.cfmac.csic.es

a few micrometers, related to the volume where the photons are diffracted. This problem can be mitigated by studying thin film samples to avoid contributions from the underlying bulk material [5, 7–9]. Perfect films are epitaxially grown and the substrate could induced strain changes that will affect the properties of a thin film [10, 11]. It is possible to get the depth sensitive information via grazing incidence [12]. But the measurement has to be performed for different incidence angles to achieve different penetration depths. That means that multiple measurement are required for a reconstruction of the crystal lattice, as the signal is an averaged for each depth [13]. And with this, the single shot measurements not possible with depth resolution.

Yet, most real-world processing applications deal with bulk materials. For example, bulk semiconductors offer not only a superior crystal quality as compared to thin films but are also of high fundamental and at least equal technological interest, owed to their dominant position in the electronics industry and silicon photonics [14]. Optical pump-probe techniques are inherently surface sensitive and have been used to confirm non-thermal melting in semiconductors [15, 16]. However, they are indirect techniques since they rely on monitoring the optical properties of materials, rather than the structural phase, which makes x-ray based techniques indispensable.

Laser-structuring bulk semiconductors with ultimate precision requires an understanding of the complex processes involved. Starting by instantaneous non-thermal melting of a surface layer of several tens of nanometers [3, 5, 17]. Followed by the inward propagation of a sharp melt-front at speeds up to a  $1 \text{ km s}^{-1}$  followed by slower interfacial re-solidification [5, 15, 18]. As well as shock wave propagation into the material [3] at propagation speeds up to  $10 \text{ km s}^{-1}$ . Therefore, an experimental tool enabling the measurement of fast and ultrafast laser-induced structural changes with high temporal, but also depth resolution, is highly desired. Early work preformed with single crystals in Bragg geometry [5, 19–21] and asymmetric Laue geometry [22], where performed at synchrotron sources, which limited the temporal resolution to about 50 ps to 100 ps (duration of the x-ray probe pulses) and making single pulse probing capability to be complex.

With the advent of x-ray Free Electron Lasers (XFELs) [23, 24], powerful structure-sensitive techniques for studying the dynamics of ultrafast processes have begun to emerge [25–28]. These techniques employ the extraordinary flux, the high spatial coherence, short wavelength and the ultrashort duration of the emitted x-ray pulses for probing ultrafast

phase transitions, permanent and transient changes of the long-range order in matter, such as strain, phonon oscillations or melting [25, 29–31]. The laser-induced changes typically contain depth-resolved information such as the strain profile of the acoustic phonons, i.e. strain waves or the strain profile due to thermal heating. Either only the averaged information is used for further data evaluation or the depth sensitive information is extracted using complex models and their output is compared with the experimental data [9, 32–34]. A more direct way of measuring the depth profile of the strain caused by these excitations would be desirable.

In recent years, Rodriguez-Fernandez and co-workers demonstrated the use of x-ray microscopy with focus x-rays to record the wavefronts from pristine single crystals [35]. Moreover, Rodriguez-Fernandez et al. presented how using a coherent diffraction imaging variant, "tele-ptychography", it is possible to sense with nanometer resolution the distorted wavefronts generated by surface strained crystals [36]. To simulate the wavefronts, they used a formalism based on the understanding of the temporal response of dynamical diffraction theory [37–40]. Ultrafast dynamical diffraction (UDD) is a process in which multiple diffracted beams, denoted as echoes, are generated at the exit surface of a crystal, both in the diffraction and forward directions [41–43]. The echoes are the constructive interference of all the x-ray beams diffracted multiple times inside the crystal in the area denoted as Borrmann fan (blue triangle in the sketch presented in Figure 1) [37, 44]. Only the x-rays that arrive to the surface of the crystal with the same phase will contribute to the formation of the UDD signal. Due to the different paths of the x-ray photons in the crystal, each of these interferences is going to exit the surface at a different time, which results in a delay with respect to the next x-ray echo of a few femtoseconds. The UDD process is a two wave interference problem where only one diffraction plane is excited by the x-rays. Due to this, all diffracted photons in all the echoes share the same properties of mono-chromaticity and divergence, and can be defined as delayed copies of the same monochromatic x-ray pulse, thus the term "echoes" in resemblance to the sound echoes. The distribution of these photon beams exiting the crystal in real space relates to the reflectivity for a particular moment in time of the crystal lattice along the depth. The entire UDD process occurs in the time that the x-ray photons need to travel through the crystal at the speed of light, e.g. 100 fs for a 30  $\mu\text{m}$  thick crystal. The measured spatial distribution of the echoes at the detector plane corresponds to a snapshot of the crystal lattice depth profile at the time in which the diffraction was collected both in the forward and in the diffraction direction. This technique

has been used so far only for measuring residual strain wavefronts at synchrotrons in perfect crystals such as diamond, Si and InSb [35, 36, 45, 46]. The spatio-temporal coupling of these echoes could be used for x-ray splitting and delay systems or future x-ray optics for attosecond sources [47]. The echoes are also expected to be observable in thin single crystals from metals as presented in [48].

In this work, we present for the first time to our knowledge the Borrmann fan of a single crystal in Laue diffraction geometry using a single femtosecond hard x-ray pulses from XFEL. Moreover, we present for first time the effect that a femtosecond pump laser has on the structure of the Borrmann fan. We use the UDD signal in a pump-probe scheme for time and depth resolved measurements of transient structural changes, induced by femtosecond laser irradiation of crystalline materials. Here, we use the relation between the detector signal intensity in the transversal direction and the depth of the crystal, as a streaking method, to study transient laser-induced strain in Silicon. We present the laser-induced transient changes of the Borrmann fan signal as a function of laser fluence and pump-probe time delay in an excitation regime below the melting threshold. Numerical calculations that combine UDD simulations with a 3D version of the model by Thomsen et al. [49] to describe the generation and propagation of ps strain pulses show good agreement with the experimental results and allow their quantitative understanding.

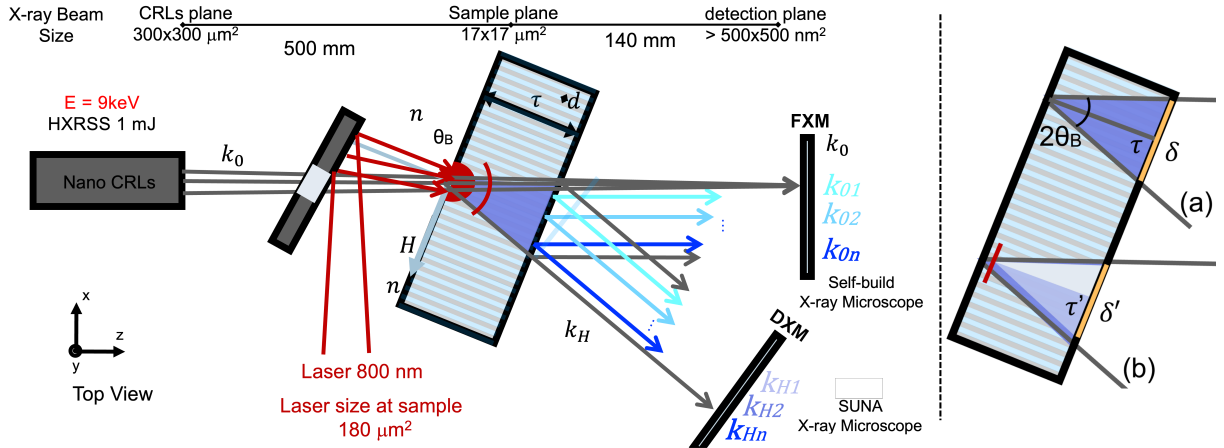


FIG. 1. (Left) Scheme of the experimental setup and (Right) Sketch of the Borrmann fan for (a) pristine and (b) distorted crystal cases. In (b) a red line represents the strain wave propagating along the crystal. A white triangle is painted to denote the area from the non distorted Borrmann fan.

## II. EXPERIMENT

The experiment was performed at the Materials Imaging and Dynamics (MID) instrument at the beamline SASE 2 of the European XFEL [50]. The undulators delivered 10 Hz self-seeded x-rays pulses at 9 keV [51]. Two Si channel cut monochromators with (220) orientation were used to monochromatize the x-ray beam and reduce the effect of a possible SASE pedestal. The x-ray beam was focused to a spot size of  $0.5 \times 0.5 \mu\text{m}^2$  (FWHM) using 10 Beryllium compound refractive lenses (CRLs) with a curvature radius of 50  $\mu\text{m}$ . Two pinholes with 300  $\mu\text{m}$  diameter located before and after the CRLs defined the numerical aperture. With these parameters the CRLs had a working distance of 640 mm. A EPIX detector was used to check for intensity fluctuations in the incoming x-ray beam. The EPIX detector was located facing to the exit window of the nano-focusing CRLs. A radiation shielding covered the EPIX detector to prevent possible x-rays coming from either upstream or downstream. In the focal plane of the CRLs, the sensitive surface of two x-ray microscopes were located, one in diffraction direction (DXM) and one in forward direction (FXM). Each of these x-ray microscopes consisted in a 20  $\mu\text{m}$  thin Ce doped GAGG scintillator crystal as x-ray sensing material, an optical magnification of 20x and a Andor Zyla 5.5 camera with a sCMOS sensor. With this configuration, each of the x-ray microscopes had an effective pixel size of around 325 nm/pixel. While the DXM was used to collect the primary signal presented in this manuscript. The FXM was used to check for possible instabilities of the x-ray position in the horizontal and vertical directions. The data from the FXM was used as a monitor to select x-ray shots with high intensity while analysing the data collected with the DXM.

The sample, a 300  $\mu\text{m}$  thin Si wafer with (001) orientation was located 500 mm downstream of the CRLs, where the x-ray beam size was of 17  $\mu\text{m}^2$ . The sample was set to diffract in the symmetrical Laue (220) reflection as shown in the experimental sketch in Figure 1(left). In this geometry, the diffraction signal is only sensitive to variations of the lattice in the component parallel to the surface of the crystal (in the direction  $H$ ), which means that we are not sensitive to the perpendicular component in which the shock or strain wave should propagate.

An optical laser with wavelength 800 nm, pulse duration 15 fs and maximum fluence of 100 mJ/cm<sup>2</sup> was used to excite the front surface of the Si sample [52]. The optical laser

travels almost collinear to the x-ray beam, using an in-coupling mirror with a 3 mm hole to allow the x-ray beam to be transmitted without distorting the wavefront. The laser passed a circular aperture of 4 mm and was focused using a lens to a near-circular spot with a measured FWHM  $w = 180 \mu\text{m}^2$ . The fluence of the laser was controlled using a rotatable half-wave plate in combination with a polarizing beam splitter that allows to adjust the incident fluence in the range from  $20 \text{ mJ}/\text{cm}^2$  to  $100 \text{ mJ}/\text{cm}^2$  [30]. For the beam waist measurement and the fluence calibration, a series of single pulse irradiation experiments on Si at fluences above the materials modification threshold were performed, as detailed in the supplementary material SM1. These measurements also allowed to quantify the melting threshold of the Si sample ( $F_m = 100 \text{ mJ}/\text{cm}^2$ ) based on the fact that ultrafast melting is followed by rapid quenching, leaving behind an amorphous mark that can be detected with optical microscopy [53, 54]. The time delay between x-rays and optical laser was scanned by an optical delay stage that allows a scan range of  $\pm 2000 \text{ ps}$  with a precision below 50 fs. A camera located after a mirror in the laser path was used to monitor the jittering and intensity stability monitor for both vertical and horizontal directions. The values from this monitor were used to select the images collected at the DXM with correct parameters of the laser pump.

### III. DISCUSSION

Figure 2(a) shows the diffraction signal recorded with DXM generated by the Si wafer in absence of laser excitation. The pattern corresponds to the so-called Borrmann fan and the intensity modulation is a result of the UDD. In the figure is illustrated the horizontal scale  $\delta$  in the detector image. As sketch in Fig. 1(right up),  $\delta$  is related to the depth  $\tau$  and can be converted using  $\delta = 2\tau \tan(\theta)$ , where  $\theta$  represents the diffraction angle. For a crystal with thickness  $\tau = 300 \mu\text{m}$  diffracting at an angle  $\theta$  of  $21.021^\circ$ ,  $\delta$  will be of  $230.58 \mu\text{m}$ . For comparison, Figure 2(b) shows the pattern recorded upon laser excitation at the front surface at a fluence  $F = 52 \text{ mJ}/\text{cm}^2$  and a pump-probe delay of  $t = 900 \text{ ps}$ . The strong effect of the laser pulse – even at fluences below the melting threshold – can be appreciated best in the horizontal profiles of the patterns depicted in Figure 2(a) and (b) for the pristine and excited crystals, respectively. While the intensity profile without pump laser in Figure 2(a') is essentially symmetric with respect to center of the wave-field, the pumped signal Figure

2(b') shows a strong decrease near the front surface and a recovery that ends with similar intensity values in the signal produced at the rear surface. To understand the distorted signal, we have to refer to the depth of the crystal in which the strain wave has not yet arrived. As represented in Figure 1(right bottom) with the white triangle. For a delay  $t = 900$  ps the strain wave will have traveled at the speed of sound to a depth of  $7.6 \mu\text{m}$ , most of the crystal ( $292.4 \mu\text{m}$ ) being not distorted. We can define a new triangle with thickness  $\tau'$  in which the crystal will be undistorted. If we calculate the surface of the Borrmann fan for this new crystal, we obtain  $\delta' = 224.76 \mu\text{m}$ . But only half of this surface will be the result of photons that have not interacted with other photons diffracted from the distorted area, yielding a non-affected Borrmann fan of  $112.38 \mu\text{m}$ . If we subtract this distance from the value obtained with the pristine crystal,  $\delta$ , we obtain an affected Borrmann fan of  $118.19 \mu\text{m}$ , which is consistent with the experimental data of the distortion signal extending to about half of the rear-illuminated area.

Due to the interference nature of the UDD mechanisms, a quantitative interpretation of the static and transient signals requires modeling. To this end, we have used the dynamical diffraction code developed for [35, 36] and introduced additionally a new laser-induced

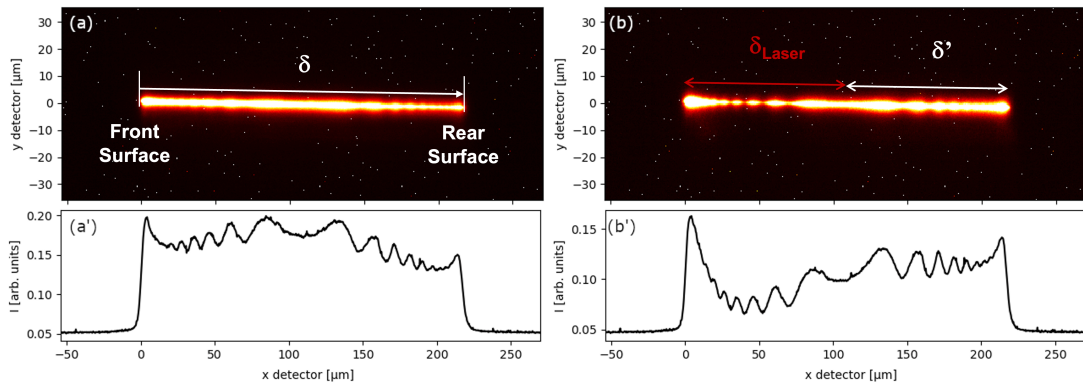


FIG. 2. Single-pulse x-ray diffraction signals of a Si  $300 \mu\text{m}$  thick crystal set to diffract for the Laue 220 symmetric reflection at  $9 \text{ keV}$  in horizontal geometry recorded by the diffraction x-ray microscope (DXM). (a) No laser incident on the sample (b) single femtosecond laser pulse at  $F = 52 \text{ mJ}/\text{cm}^2$ ,  $900 \text{ ps}$  before the x-ray probe pulse. The labels indicate the positions of the front and rear surface of the Si wafer, illustrating the capability of depth-resolved measurements. (a') and (b') are the horizontal profiles of the diffracted signal along the horizontal detector direction, from (a) and (b), respectively.



strain model based on the analytical solution of the Thomsen model [49]. In our model, we assume a radial system with two components, a component perpendicular to the surface of the crystal for which a bipolar strain wave propagates and a parallel component in which a radial gaussian-like strain wave propagates. Each of these deformation waves propagates at different speeds,  $8.4 \text{ km s}^{-1}$  for the longitudinal and  $5.8 \text{ km s}^{-1}$  for the transversal contributions, respectively. This allows us to simulate the diffracted signal, as described in more detail in the supplementary material, section 1. Figure 3 presents the simulations performed with the dynamical diffraction code for the same conditions as in Fig 2. We can observe the same signal length  $230 \mu\text{m}$  for both simulated and experimental data. The simulated data has more fringes near the edge of the signal, which we related to a possible inhomogeneities of the crystal sample in the surfaces and the big x-ray beam of  $17 \mu\text{m}$  and the effect of the curve x-ray wavefront on the sample. In previous studies performed at a synchrotron in which the sample is located at the focus a better match was observed [36]. In the case of the pump sample Fig. 3(b), the simulated signal present the same depression as observed in the experimental data. In the front surface, the first maxima is more intense than the one observed in the experimental data, if we compared with the overall intensity of the signal, but the length of the distorted signal matches the one of the experimental data.

Figure 4 displays a series of simulated diffraction profiles for the experimental conditions

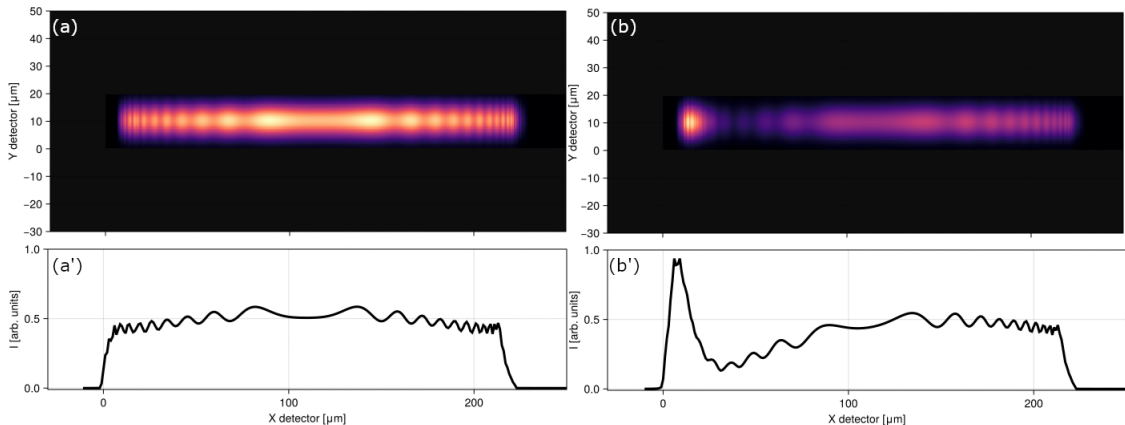


FIG. 3. Simulations of two diffraction wavefronts for a Si  $300 \mu\text{m}$  thick crystal set to diffract in the symmetric Laue (220) reflection at  $9 \text{ keV}$  (a) no laser and (b)  $900 \text{ ps}$  after a  $800 \text{ nm}$   $15 \text{ fs}$  laser with a fluence of  $50 \text{ mJ/cm}^2$  incident on the front surface. (a) and (b) Profiles along the x detector direction for the wavefronts calculated in (a) and (b), respectively.

used in Fig. 2 (probe delay  $t = 900$  ps,  $F = 50$  mJ/cm<sup>2</sup>) for different laser absorption depth values in the range from 100 nm to 3  $\mu$ m. This exploration of the laser absorption depth as a parameter is necessary due to the complex laser absorption mechanism of 800 nm ultrashort laser pulses in silicon. Although at this wavelength above-bandgap excitation with a linear optical penetration depth of  $d = 10$   $\mu$ m might be assumed. But it has been shown, for instance, that dominant two-photon absorption occurs at excitation wavelengths as short as  $\lambda = 620$  nm [55]. In order to avoid our results and their interpretation to be affected by the vivid ongoing debate on the exact absorption mechanisms and dynamics that also depend on the fluence used. We have opted to incorporate in our model an effective absorption depth. The correct value for our experimental conditions is determined by using it as a fitting parameter to obtain the best match of the calculated to the experimental diffraction signal profiles. Comparing the calculated curves in Fig. 4 to the experimental profiles as presented in Figure 2 (b') we conclude that the best match is obtained for an effective laser absorption depth of  $d = (300 \pm 100)$  nm.

As a next step, we have investigated the influence of the laser fluence on the lattice distortions, leaving the delay constant at  $t = 900$  ps. The fluence range explored was from 20 mJ/cm<sup>2</sup> to 100 mJ/cm<sup>2</sup>. The experimental profiles are shown in Figure 5 (left column). A progressive decrease of the x-ray signal amplitude with fluence throughout the entire material thickness, but strongest near the front surface, can be observed. We define the experimental melting threshold as  $F_m = (100 \pm 10)$  mJ/cm<sup>2</sup>. As it can be observe in the lower profile of Fig. 5 for this fluence there is a high change in the inclination of the intensity of the signal profile and the position of the inner maxima have changed, what could relate

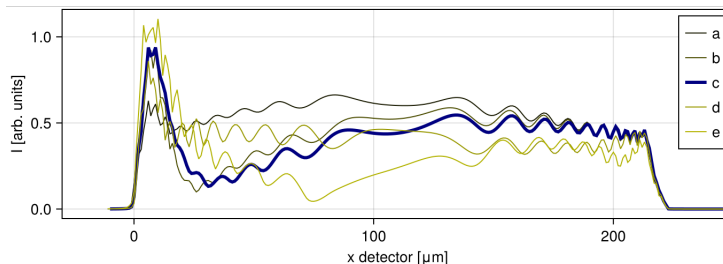


FIG. 4. Simulated depth profiles of the diffraction signal for a 800 nm laser irradiation at  $F = 50$  mJ/cm<sup>2</sup> with a delay of 900 ps between optical laser and x-ray pulses for different effective absorption lengths (a)100 nm, (b)300 nm, (c)500 nm, (d)1  $\mu$ m and (e) 3  $\mu$ m.

to a change in the thickness of the materials. Looking to the supplementary material SM1, we can also observe how for this fluence range we can observe some amorfization of the surface. We have calculated the profiles corresponding to the individual fluences using our model, the results presented in Figure 5 (right column). Overall, the same trend as observed experimentally, the progressive signal reduction near the front surface, is well reproduced. However, the calculations for  $F = 20 \text{ mJ/cm}^2$  and  $F = 36 \text{ mJ/cm}^2$  predict a much stronger suppression than observed experimentally. Looking in more detail, it can be seen that the simulation for  $F = 20 \text{ mJ/cm}^2$  matches better the experimental results for  $F = 36 \text{ mJ/cm}^2$  fluence. A similar behavior is shown in Figure SM2, where we compare the simulations for  $10 \text{ mJ/cm}^2$  to experimental profiles at several fluences, obtaining a satisfactory match for  $F = 20 \text{ mJ/cm}^2$ . Likewise, the simulation for  $F = 40 \text{ mJ/cm}^2$  shows a better match to the

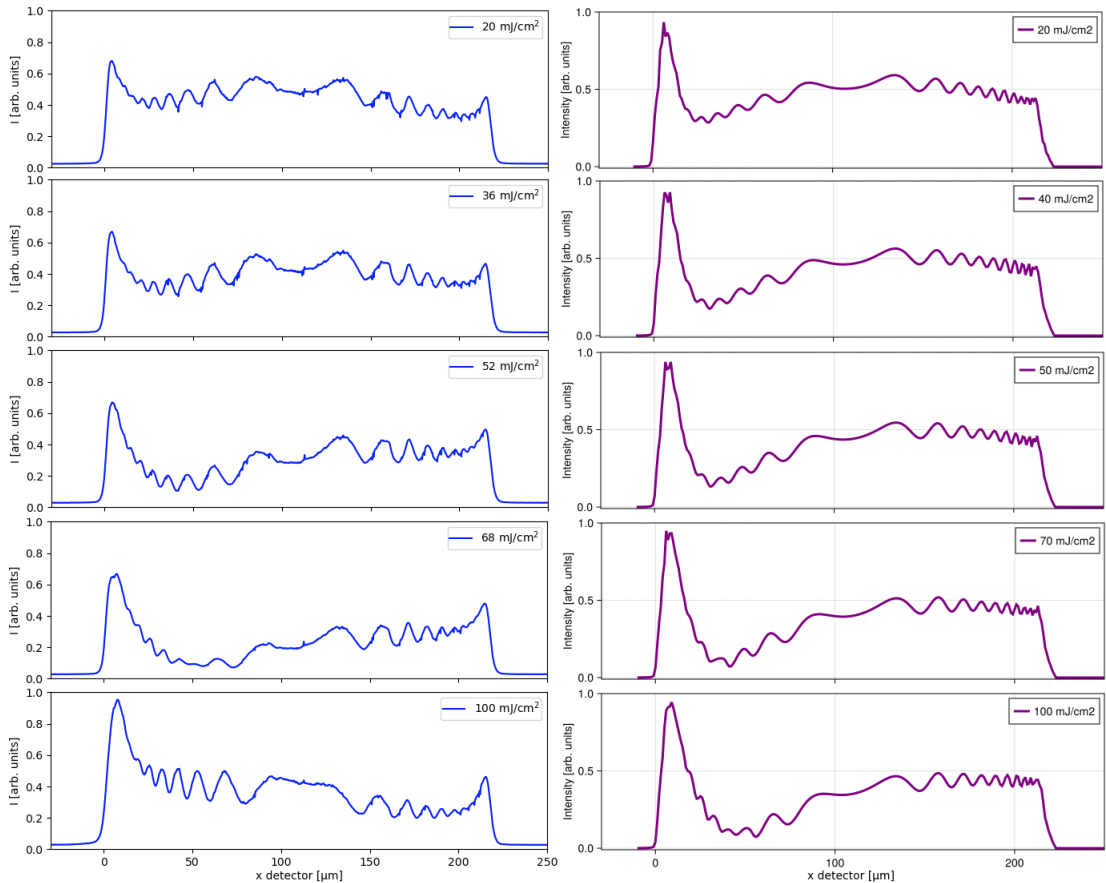


FIG. 5. (Left) Experimental profiles of the diffracted x-ray signal excited by the pump laser at an x-ray delay of 900 ps with respect to laser pump for 5 different fluences. (Right) Corresponding simulations for the same experimental conditions.

experimental results for  $F = 52 \text{ mJ/cm}^2$ . This behavior is indicative of a reduced energy deposition at low fluences, which is consistent with the presence of a non-linear absorption mechanism and might be influenced by our current approximation, employing the same effective absorption depth (300 nm) for the fluence range studied. While the results shown above for fluences up to  $70 \text{ mJ/cm}^2$  demonstrate a good agreement of the model with the experimental data, for higher fluences a poor match is observed. We attribute this to a number of mechanisms, including a different non-linear absorption regime, nucleation of the liquid phase, changes in the sample reflectivity during absorption due to the high free carrier density, among others.

Besides the laser fluence, the delay time between pump and probe beam is expected to strongly affect the recorded signal and to allow unraveling the strain wave propagation dynamics. A waterplot of the experimental profiles for a delay range of  $t = -100 \text{ ps}$  to  $900 \text{ ps}$  are plotted in Figure 6(left), featuring a near-surface signal depression whose amplitude increases with time and whose position moves along the crystal depth (most pronounced in the range from 300 ps to 900 ps). Qualitatively, the same trend can be observed in the simulated profiles presented in Figure 6 (right). However, an important difference is the strong signal increase at the front surface predicted at long delays, which is less pronounced in the experimental data. Some particular profiles at different delay time between laser pump and x-ray probe for the experimental and simulated signals are presented in Figure SM3 in the supplementary material.

In the previous work by Lings and co-workers [22], conventional TR-XRD was used in

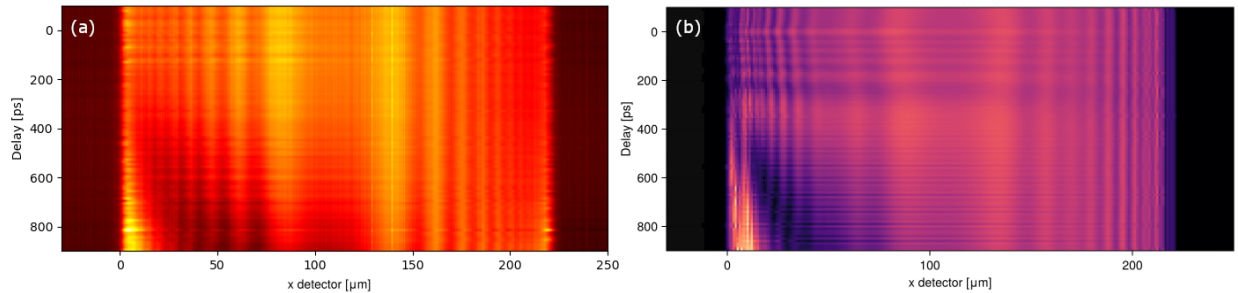


FIG. 6. (Left) Water plot of the experimental profiles of the diffraction signal upon excitation at  $F = 52 \text{ mJ/cm}^2$  as a function of pump-probe delay times from  $-100 \text{ ps}$  to  $900 \text{ ps}$ . (Right) Waterplot of the corresponding simulated profiles using  $F = 50 \text{ mJ/cm}^2$  and a laser penetration depth  $d = 300 \text{ nm}$ .

Laue geometry to study the effect of a pump laser on the asymmetric Ge ( $20\bar{2}$ ) reflection at a synchrotron. The authors neglected the contribution of the parallel component of the lattice distortion after the laser pulse, assuming that the longitudinal component is the only one observable. In our opinion, this explains the poor match between simulations and experimental results the authors observed, as both components contribute to the signal. In the specific reflection we have chosen for the present study, we are only sensitive to the parallel component of the lattice distortion. The good agreement between the simulations and the experimental data in our study, at least for short delays, suggests that the contribution of the parallel component it is not neglectable as proposed in [22]. This motivates our further interest in performing experiments in the same geometrical conditions as Lings and co-workers in order to detect and resolve both lattice distortion components.

#### IV. CONCLUSIONS

We have presented experimental single-pulse, ultrafast pump-probe data of the Bormann fan distribution in crystalline Si upon NIR fs laser excitation at an XFEL source. The obtained ultrafast dynamical diffraction signal is based on spatio-temporal coupling and can be used to understand complex ultrafast processes such as lattice distortions and their temporal evolution inside bulk single crystals. Already at a delay of 50 ps, we observe a clear response from the crystal for the symmetric Laue (220) reflection. Moreover, we have developed a model based on the Thomsen analytical model that is able to fit the experimental data for short delays and fluences below the melting threshold. The model fits reasonably well the experimental data collected at a laser fluence of  $52 \text{ mJ/cm}^2$ , using an effective absorption depth of 300 nm as a single fit parameter. Future modelling work will be focused on extending the model for long delays and high fluences. This new experimental method has the potential to provide relevant information about the stress that x-ray optics suffer after femtosecond/attosecond x-ray pulse irradiation of the surface of a crystal in diffraction condition. Due to the high sensitivity of the UDD-signal to the lattice distortions along the crystal depth, this method can help to unveil ultrafast processes at higher fluences, such as ultrafast melting, ablation and shock wave generation, present upon femtosecond laser processing of single-crystal semiconductors and metals. Employing this knowledge, optimized laser fabrication of 3D structures can be achieved, increasing the quality and

efficiency of industrial semiconductor manufacturing and reducing the costs by avoiding undesired damage.

## **ACKNOWLEDGMENTS**

We acknowledge European XFEL in Schenefeld, Germany, for provision of x-ray free-electron laser beamtime at MID and would like to thank the staff for their assistance. Data recorded for the experiment at the European XFEL are available at doi: 10.22003/XFEL.EU-DATA-004977-00. This research was supported in part through the Maxwell computational resources operated at Deutsches Elektronen-Synchrotron DESY, Hamburg, Germany. This work was partly funded by the Consejera de Educacin, Ciencia y Universidades (Comunidad de Madrid, (Spain)) through the MATRIX-CM project (TEC-2024/TEC-85) and by MCIN/AEI/10.13039/501100011033 through HyperSpec grant (PID2023-148178OB-C22). This work was supported by ERC-2020-STG, 3DX-FLASH (948426). DK, TJA, and KST acknowledge by the Deutsche Forschungsgemeinschaft (DFG, German Research Foundation) through Project 638 No. 278162697-SFB 1242. The access to the European XFEL was supported by a grant of the Polish Ministry of Science and Higher Education- decision no. 2022/WK/13. This work was supported by the National Science Centre, Poland, grant agreement No 2021/43/B/ST5/02480. We would like to thank J. Domagala for the support in the pre-characterization of the samples. One of us would like to thank K. Finkelstein for many hours of discussion about dynamical diffraction and showing the first steps in the world of pump-probe in single crystals. One of us would like to thank G. Carbone, U. Staub, A. Diaz, for the fruitful discussion in relation with the imaging of ultrafast wavefronts. We would like to thank the discussion about dynamical diffraction with L. Horak, L Samoylova and I. Petrov.

## **Appendix A: Appendixes**

### **1. Analytical Thomsen model**

Thomsen et al. proposed an analytical 1D model to describe the generation of a stress pulse in a crystalline material after laser excitation [49]. The model uses the optical, electronic and acoustic properties of the material to represent the lattice distortion at different time

delays. Following the model, the strain in the perpendicular direction to the surface  $\eta_{33}$  in a material as a function of depth  $z$  and delay time  $t$  would be:

$$\eta_{33} = (1 - R) \frac{Q\beta}{A\zeta C} \left[ e^{-\frac{z}{\zeta}} \left( 1 - \frac{1}{2} e^{-\frac{v_L t}{\zeta}} \right) - \frac{1}{2} e^{-\frac{|z-v_L t|}{\zeta}} \text{sgn}(z - v_L t) \right] \quad (\text{A1})$$

where  $v_L$  is the longitudinal sound velocity,  $R$  the reflectivity of the material,  $Q$  the laser fluence,  $A$  the illuminated area,  $\beta$  the linear expansion coefficient,  $C$  is the specific heat per unit volume,  $\zeta$  is the absorption length and  $\nu$  the Poisson ratio.

In a similar way, we can describe the lattice displacement parallel to the surface in a radial form as presented in eq. (A2). In the parallel direction, we do not expect to observe a bipolar function propagating. This displacement will be slower with respect to the perpendicular strain wave propagating on the crystal, as  $v_L$  is the transversal sound velocity in the material. And extra radial factor can be used to modulate the intensity of the lattice distortion as a function of the distance to the center of the laser impact.

$$\eta_{pp} = (1 - R) \frac{Q\beta}{A\zeta C} \left[ e^{-\frac{z}{\zeta}} \left( 1 - \frac{1}{2} e^{-\frac{v_T t}{\zeta}} \right) - \frac{1}{2} e^{-\frac{|z-v_T t|}{\zeta}} \right] \quad (\text{A2})$$

Figure 7 shows the simulated lattice distortion for a time delay of 800 ps produced by a 50 mJ/cm<sup>2</sup>, 800 nm femtosecond laser pulse that excites the front surface of a Si crystal for

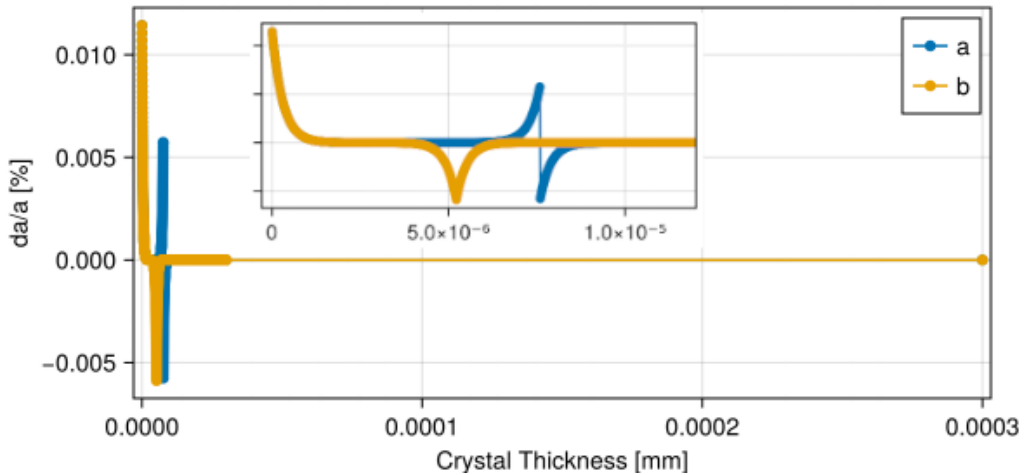


FIG. 7. (a) Simulated depth profile along the perpendicular direction to the surface crystal following the analytical solution presented in eq. A1 [49]. (b) Simulated depth profile along the parallel direction to the surface crystal as a function of depth following the analytical solution presented in eq. (A2)

both the perpendicular (a) and parallel (b) directions. For it we have used the solution in eq.A1 and our proposed approximation for the parallel direction is presented in eq. A2.

- 
- [1] M. Chambonneau, D. Grojo, O. Tokel, F. o. Ilday, S. Tzortzakis, and S. Nolte, In-volume laser direct writing of silicon challenges and opportunities, *Laser & Photonics Reviews* **15**, 2100140 (2021).
  - [2] R. Stoian and J.-P. Colombier, Advances in ultrafast laser structuring of materials at the nanoscale, *Nanophotonics* **9**, 4665 (2020).
  - [3] T. Zier, E. S. Zijlstra, A. Kalitsov, I. Theodonis, and M. E. Garcia, Signatures of nonthermal melting, *Structural Dynamics* **2**, 054101 (2015).
  - [4] C. W. Siders, A. Cavalleri, K. Sokolowski-Tinten, C. Tth, T. Guo, M. Kammler, M. H. von Hoegen, K. R. Wilson, D. von der Linde, and C. P. J. Barty, Detection of nonthermal melting by ultrafast x-ray diffraction, *Science* **286**, 1340 (1999).
  - [5] K. Sokolowski-Tinten, C. Blome, C. Dietrich, A. Tarasevitch, M. Horn von Hoegen, D. von der Linde, A. Cavalleri, J. Squier, and M. Kammler, Femtosecond x-ray measurement of ultrafast melting and large acoustic transients, *Phys. Rev. Lett.* **87**, 225701 (2001).
  - [6] A. Rousse, C. Rischel, S. Fourmaux, I. Uschmann, S. Sebban, G. Grillon, P. Balcou, E. Förster, J. Geindre, P. Audebert, J. Gauthier, and D. Hulin, Non-thermal melting in semiconductors measured at femtosecond resolution, *Nature* **410**, 65 (2001).
  - [7] A. M. Lindenberg, S. Engemann, K. J. Gaffney, K. Sokolowski-Tinten, J. Larsson, P. B. Hillyard, D. A. Reis, D. M. Fritz, J. Arthur, R. A. Akre, M. J. George, A. Deb, P. H. Bucksbaum, J. Hajdu, D. A. Meyer, M. Nicoul, C. Blome, T. Tschentscher, A. L. Cavalieri, R. W. Falcone, S. H. Lee, R. Pahl, J. Rudati, P. H. Fuoss, A. J. Nelson, P. Krejcik, D. P. Siddons, P. Lorazo, and J. B. Hastings, X-ray diffuse scattering measurements of nucleation dynamics at femtosecond resolution, *Phys. Rev. Lett.* **100**, 135502 (2008).
  - [8] J. Pudell, A. A. Maznev, M. Herzog, M. Kronseder, C. H. Back, G. Malinowski, A. Reppert, and M. Bargheer, Layer specific observation of slow thermal equilibration in ultrathin metallic nanostructures by femtosecond X-ray diffraction, *Nature Communications* **9**, 3335 (2018).
  - [9] W. Jo, J. Kee, K. Kim, E. C. Landahl, G. Longbons, D. A. Walko, H. Wen, D. R. Lee, and S. Lee, Structural measurement of electron-phonon coupling and electronic thermal transport



- across a metal-semiconductor interface, *Scientific Reports* **12**, 16606 (2022).
- [10] W. Lu, W. Song, P. Yang, J. Ding, G. M. Chow, and J. Chen, Strain Engineering of Octahedral Rotations and Physical Properties of SrRuO<sub>3</sub> Films, *Scientific reports* **5**, 10245 (2015), num Pages: 9.
- [11] I. Vrejoiu, M. Alexe, D. Hesse, and U. Gösele, Functional Perovskites - From Epitaxial Films to Nanostructured Arrays, *Adv. Funct. Mater.* **18**, 38923906 (2008).
- [12] M. Trigo, M. Fuchs, J. Chen, M. P. Jiang, M. Cammarata, S. Fahy, D. M. Fritz, K. Gaffney, S. Ghimire, A. Higginbotham, S. L. Johnson, M. E. Kozina, J. Larsson, H. Lemke, A. M. Lindenberg, G. Ndabashimiye, F. Quirin, K. Sokolowski-Tinten, C. Uher, G. Wang, J. S. Wark, D. Zhu, and D. A. Reis, Fourier-transform inelastic X-ray scattering from time- and momentum-dependent phononphonon correlations, *Nature Physics* **9**, 790 (2013).
- [13] D. A. Walko, Y.-M. Sheu, M. Trigo, and D. A. Reis, Thermal transport in thin films measured by time-resolved, grazing incidence x-ray diffraction, *Journal of Applied Physics* **110**, 102203 (2011).
- [14] V. Almeida, C. Barrios, R. Panepucci, and et al., All-optical control of light on a silicon chip, *Nature* **431**, 10811084 (2004).
- [15] N. Casquero, C. R. de Galarreta, Y. Fuentes-Edfuf, J. Solis, C. D. Wright, and J. Siegel, Propagation dynamics of the solidliquid interface in ge upon ns and fs laser irradiation, *Journal of Physics D: Applied Physics* **55**, 365104 (2022).
- [16] K. Sokolowski-Tinten, J. Bialkowski, M. Boing, A. Cavalleri, and D. von der Linde, Thermal and nonthermal melting of gallium arsenide after femtosecond laser excitation, *Phys. Rev. B* **58**, R11805 (1998).
- [17] B. Rethfeld, D. S. Ivanov, M. E. Garcia, and S. I. Anisimov, Modelling ultrafast laser ablation, *Journal of Physics D: Applied Physics* **50**, 193001 (2017).
- [18] H. Hu, X. Wang, H. Zhai, N. Zhang, and P. Wang, Generation of multiple stress waves in silica glass in high fluence femtosecond laser ablation, *Appl. Phys. Lett.* **97**, 061117 (2010).
- [19] B. C. Larson, C. W. White, T. S. Noggle, and D. Mills, Synchrotron x-ray diffraction study of silicon during pulsed-laser annealing, *Phys. Rev. Lett.* **48**, 337 (1982).
- [20] J. Z. Tischler, B. C. Larson, and D. M. Mills, Timeresolved xray study of Ge during pulsed laser melting, *Applied Physics Letters* **52**, 1785 (1988).
- [21] M. F. DeCamp, D. A. Reis, D. M. Fritz, P. H. Bucksbaum, E. M. Dufresne, and R. Clarke,

- X-ray synchrotron studies of ultrafast crystalline dynamics, *Journal of Synchrotron Radiation* **12**, 177 (2005).
- [22] B. Lings et al., Simulations of time-resolved x-ray diffraction in laue geometry, *J. Phys.: Condens. Matter* **18**, 92319244 (2006).
- [23] J. M. Glowia et al., Time-resolved pump-probe experiments at the lcls, *Opt. Express* **18**, 17620 (2010).
- [24] W. Decking et al., A mhz-repetition-rate hard x-ray free-electron laser driven by a superconducting linear accelerator, *Nat. Photonics* **14**, 391 (2020).
- [25] M. Trigo, A. Bruchhausen, A. Fainstein, B. Jusserand, and V. Thierry-Mieg, Confinement of acoustical vibrations in a semiconductor planar phonon cavity, *Phys. Rev. Lett.* **89**, 227402 (2002).
- [26] P. Zalden, F. Quirin, S. J. S. Wei, A. Koc, M. Nicoul, M. Trigo, P. Andreasson, H. Enquist, M. J. Shu, T. Pardini, M. Chollet, D. Zhu, H. Lemke, I. Ronneberger, J. Larsson, A. M. Lindenberg, H. E. Fischer, S. Hau-Riege, D. A. Reis, R. Mazzarello, M. Wuttig, and K. Sokolowski-Tinten, Femtosecond x-ray diffraction reveals a liquid-liquid phase transition in phase-change materials, *Science* **364**, 1032 (2019).
- [27] L. E. Dresselhaus-Marais, B. Kozioziemski, T. S. Holstad, T. M. Rder, M. Seaberg, D. Nam, S. Kim, S. Breckling, S. Choi, M. Chollet, P. K. Cook, E. Folsom, E. Galtier, A. Gonzalez, T. Gorkhover, S. Guillet, K. Haldrup, M. Howard, K. Katagiri, S. Kim, S. Kim, S. Kim, H. Kim, E. B. Knudsen, S. Kuschel, H. J. Lee, C. Lin, R. S. McWilliams, B. Nagler, M. M. Nielsen, N. Ozaki, D. Pal, R. Pablo Pedro, F. Saunders, Alison M. and Schoofs, T. Sekine, H. Simons, T. van Driel, B. Wang, W. Yang, C. Yildirim, H. F. Poulsen, and J. H. Eggert, Simultaneous bright- and dark-field x-ray microscopy at x-ray free electron lasers, *Scientific Reports* **13**, 17573 (2023).
- [28] S. J. Irvine, K. Katagiri, T. M. Rder, U. Boesenberg, D. Chalise, J. I. Stanton, D. Pal, J. Hallmann, G. Ansaldi, F. Braue, J. H. Eggert, L. Fang, E. Folsom, M. Haubro, T. S. Holstad, A. Madsen, J. Möller, M. M. Nielsen, H. F. Poulsen, J.-E. Pudell, A. Rodriguez-Fernandez, F. Schoofs, F. Seiboth, Y. Wang, W. Jo, M. Youssef, A. Zozulya, K. Haldrup, and L. E. Dresselhaus-Marais, Dark-field x-ray microscopy for 2d and 3d imaging of microstructural dynamics at the european x-ray free-electron laser, *Journal of Applied Physics* **137**, 053106 (2025).

- [29] R. Alonso-Mori et al., Achieving few-femtosecond time-sorting at hard x-ray free-electron lasers, *J. Synchrotron Radiat.* **22**, 612 (2015).
- [30] R. Shayduk, J. Hallmann, A. Rodriguez-Fernandez, M. Scholz, W. Lu, U. Bösenberg, J. Möller, A. Zozulya, M. Jiang, U. Wegner, R.-C. Secareanu, G. Palmer, M. Emons, M. Lederer, S. Volkov, I. Lindfors-Vrejoiu, D. Schick, M. Herzog, M. Bargheer, and A. Madsen, Femtosecond x-ray diffraction study of multi-thz coherent phonons in srtio3, *Applied Physics Letters* **120**, 202203 (2022).
- [31] J. Antonowicz, A. Olczak, K. Sokolowski-Tinten, P. Zalden, I. Milov, P. Dzigielewski, C. Bressler, H. N. Chapman, M. Chojnacki, P. Duewski, A. Rodriguez-Fernandez, K. Fronc, W. Gaweda, K. Georganakis, A. L. Greer, I. Jacyna, R. W. van de Kruijs, R. Kamiski, D. Khakhulin, D. Klinger, K. M. Kosyl, K. Kubicek, K. P. Migdal, R. Minikayev, N. T. Panagiotopoulos, M. Sikora, P. Sun, H. Yousef, W. Zajkowska-Pietrzak, V. V. Zhakhovsky, and R. Sobierajski, Structural pathways for ultrafast melting of optically excited thin polycrystalline palladium films, *Acta Materialia* **276**, 120043 (2024).
- [32] J. Pudell, M. Mattern, M. Hehn, G. Malinowski, M. Herzog, and M. Bargheer, Heat transport without heating? – an ultrafast x-ray perspective into a metal heterostructure, *Advanced Functional Materials* **30**, 2004555 (2020).
- [33] W. Jo, F. Westermeier, R. Rysov, O. Leupold, F. Schulz, S. Tober, V. Markmann, M. Sprung, A. Ricci, T. Laurus, A. Aschkan, A. Klyuev, U. Trunk, H. Graafsma, G. Grübel, and W. Roseker, Nanosecond X-ray photon correlation spectroscopy using pulse time structure of a storage-ring source, *IUCrJ* **8**, 124 (2021).
- [34] M. Mattern, A. von Reppert, S. P. Zeuschner, M. Herzog, J.-E. Pudell, and M. Bargheer, Concepts and use cases for picosecond ultrasonics with x-rays, *Photoacoustics* **31**, 100503 (2023).
- [35] A. Rodriguez-Fernandez et al., Spatial displacement of forward-diffracted x-ray beams by perfect crystals, *Acta Cryst. A* **74**, 75 (2018).
- [36] A. Rodriguez-Fernandez, A. Diaz, A. H. S. Iyer, M. Vezhvak, K. Wakonig, M. H. Colliander, and D. Carbone, Imaging ultrafast dynamical diffraction wave fronts in strained si with coherent x rays, *Phys. Rev. Lett.* **127**, 157402 (2021).
- [37] G. Borrmann, Die absorption von röntgenstrahlen im fall der interferenz, *Zeitschrift für Physik* **127**, 297 (1950).

- [38] S. Takagi, Dynamical theory of diffraction applicable to crystals with any kind of small distortions, *Acta. Cryst.* **15**, 1311 (1962).
- [39] B. Batterman and H. Cole, Dynamical diffraction of x-rays by perfect crystals, *Reviews of Modern Physics* **36**, 681 (1964).
- [40] A. Authier, *Dynamical theory of X-ray diffraction* (Oxford University Press, 2001).
- [41] V. A. Bushuev, Diffraction of x-ray free-electron laser femtosecond pulses on single crystals in the bragg and laue geometry, *J. Synchrotron Rad.* **15**, 495 (2008).
- [42] Y. Shvydko and R. Lindberg, Spatiotemporal response of crystals in x-ray bragg diffraction, *Phys. Rev. ST Accel. Beams* **15**, 100702 (2012).
- [43] X. Yang and Y. Shvydko, Maximizing spectral flux from self-seeding hard x-ray free electron lasers, *Phys. Rev. ST Accel. Beams* **16**, 120701 (2013).
- [44] A. Authier, Optical properties of X-rays – dynamical diffraction, *Acta Crystallographica Section A* **68**, 40 (2012).
- [45] M. Vezhvak, S. Van Petegem, A. Rodriguez-Fernandez, P. Godard, K. Wakonig, D. Karpov, V. L. R. Jacques, A. Menzel, L. Thilly, and A. Diaz, X-ray ptychographic topography: A robust nondestructive tool for strain imaging, *Phys. Rev. B* **103**, 144107 (2021).
- [46] M. Carlsen, C. Detlefs, C. Yildirim, T. Ræder, and H. Simons, Simulating dark-field X-ray microscopy images with wavefront propagation techniques, *Acta Crystallographica Section A* **78**, 482 (2022).
- [47] I. Petrov, A. Buzmakov, A. Rodriguez-Fernandez, L. Samoylova, H. Sinn, and A. Madsen, Simulation of wavefront propagation in diffraction of XFEL beams by single crystals, in *Advances in Computational Methods for X-Ray Optics V*, Vol. 11493, edited by O. Chubar and K. Sawhney, International Society for Optics and Photonics (SPIE, 2020) p. 114930U.
- [48] A. Rodriguez-Fernandez, Ultrafast dynamical diffraction with nanobeams, simulations on thin Au crystals, in *X-Ray Nanoimaging: Instruments and Methods VI*, Vol. 12698, edited by B. Lai and A. Somogyi, International Society for Optics and Photonics (SPIE, 2023) p. 1269808.
- [49] C. Thomsen, H. T. Grahn, H. J. Maris, and J. Tauc, Surface generation and detection of phonons by picosecond light pulses, *Phys. Rev. B* **34**, 4129 (1986).
- [50] A. Madsen, J. Hallmann, G. Ansaldi, T. Roth, W. Lu, C. Kim, U. Boesenberg, A. Zozulya, J. Möller, R. Shayduk, M. Scholz, A. Bartmann, A. Schmidt, I. Lobato, K. Sukharnikov, M. Reiser, K. Kazarian, and I. Petrov, Materials Imaging and Dynamics (MID) instrument at

- the European X-ray Free-Electron Laser Facility, *Journal of Synchrotron Radiation* **28**, 637 (2021).
- [51] S. Liu, C. Grech, M. Guetg, and et al., Cascaded hard x-ray self-seeded free-electron laser at megahertz repetition rate, *Nat. Photon.* **17**, 984991 (2023).
- [52] G. Palmer, M. Kellert, J. Wang, M. Emons, U. Wegner, D. Kane, F. Pallas, T. Jezynski, S. Venkatesan, D. Rompotis, E. Brambrink, B. Monoszlai, M. Jiang, J. Meier, K. Kruse, M. Pergament, and M. J. Lederer, Pump-probe laser system at the FXE and SPB/SFX instruments of the European X-ray Free-Electron Laser Facility, *Journal of Synchrotron Radiation* **26**, 328 (2019).
- [53] J. Bonse and et al., All-optical characterization of single femtosecond laser-pulse-induced amorphization in silicon, *Applied Physics A* **84**, 63 (2006).
- [54] M. Garcia-Lechuga, N. Casquero, J. Siegel, J. Solis, R. Clady, A. Wang, O. Utza, and D. Grojo, Amorphization and ablation of crystalline silicon using ultrafast lasers: Dependencies on the pulse duration and irradiation wavelength, *Laser & Photonics Reviews* **18**, 2301327 (2024).
- [55] K. Sokolowski-Tinten and D. von der Linde, Generation of dense electron-hole plasmas in silicon, *Phys. Rev. B* **61**, 2643 (2000).